Computational Analysis of Tsunami Wave Behaviour for Three Historical Tsunami Events using T-Impulse Model

SYED MOHAMED E.[1], PON SELVAN C. M.[2]
[1]Department of Computer Science & Engineering,
B. S. Abdur Rahman Crescent Institute of Science and Technology,
Chennai,
INDIA

[2]Curtin University,
Dubai,
UAE

Abstract: - Natural catastrophes pose a serious threat to both human life and the environment because they are unpredictable. One of the most devastating natural disasters is a tsunami, and forecasting models are essential to preventing catastrophic damage to the environment and people along the coast. In the Impulse model, the generation of a tsunami depends on the impulse force generated during the event. Understanding tsunamis begins with simulating the tsunami generation process. This process involves simulating both the motion of the seafloor and the subsequent motion of the water above for tsunamis caused by underwater earthquakes. This modeling strategy can mimic all three stages of a tsunami: generation, propagation, and run-up. Three separate earthquake tsunami events—the 1755 Lisbon earthquake, the 1964 Alaska earthquake, the 2004 Sumatra earthquake are each investigated in this research. To demonstrate its relevance to current events and various ocean locations, the results of these events are compared and confirmed with the observed data. Analyzing the parameters used in this modeling study and identifying the parameter that has the most influence will demonstrate their significance in tsunami generation. The seabed displacement profile, seawater deformation, changes in tsunami characteristics during propagation, the tsunami's travel time, earliest arrival time, the tsunami wave height at the coast, and inundation distance are the anticipated findings from this study. The major objective of this study is to obtain the maximum and most accurate result possible using the fewest parameters possible.

Key-Words: - Impulse modelling, Tsunami wave, Fault slip variation, Fault boundary, Tsunami travel time, Fault boundary, 1755 Lisbon tsunami, 1964 Alaska tsunami, 2004 Sumatra tsunami.

Received: March 13, 2023. Revised: November 27, 2023. Accepted: December 7, 2023. Published: December 31, 2023.

1 Introduction

More than 70% of the Earth's surface is covered by water, and underwater disruptions resulting from earthquakes, landslips, volcanic eruptions, or meteorite impacts can lead to tsunamis, posing significant risks to human life and the environment, [1]. The behavior of tsunami waves can be predicted using tsunami wave modeling, which is crucial for taking precautions to protect lives from severe harm.

Although tsunamis are a common natural occurrence worldwide, they most frequently happen in the Pacific Ocean due to seismic and volcanic activity associated with tectonic plate boundaries in the Pacific Ring of Fire. The earliest known tsunami occurred around 479 BC when a Persian army advancing on the Greek town of Potidaea was wiped out, [2]. While thousands of tsunamis have been documented throughout history, the 2004 Sumatra-Andaman tsunami, which affected more than 15 nations, is considered the deadliest tsunami ever.

In this analysis, we considered three historical tsunami events covering three oceanic regions (Atlantic Ocean, Indian Ocean, Pacific Ocean) and three continents (Asia, Europe, North America,). We focused on historical earthquake-generated tsunami events: the 1755 Lisbon tsunami, [3], 1964 Alaska tsunami, [4], [5], 2004 Sumatra tsunami, [6]. Figure 1 displays the bathymetry profile of the world's oceans.

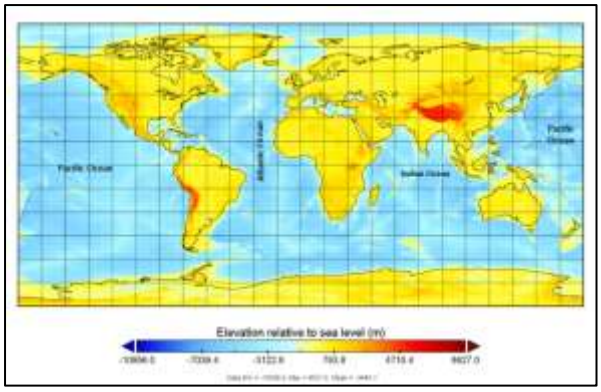

Fig. 1: Bathymetry elevation profile in the worldwide (NOAA)

In this study, the impulse model was employed to evaluate all three stages of the tsunami. The generation phase was simulated using seismic information on the impulse force produced during the earthquake. The tsunami propagation phase was constructed with the aid of the Boussinesq approximation and solitary wave theory, [7]. During this phase, the complete spectrum of tsunami characteristic changes was evaluated along the wave propagation path. The link between the direction of propagating waves and the topography of the beach was used to design the final run-up phase.

The modeling provides the tsunami's earliest arrival time based on the close distance of the source and destination locations. These results are attained due to factors such as tsunami wave propagation characteristics, seabed displacement, wave height at the coast, tsunami travel duration, and the tsunami's earliest arrival time, all influencing how a tsunami behaves.

The 1964 Alaska earthquake, with a moment magnitude of Mw = 9.2, surpassed all previous records for size, [8], [9]. Early calculations placed the rupture's length, parallel to the Alaska-Aleutian trench's strike, between 600 and 800 km, [10], [11] and its rupture velocity, [12], [13], between 3 and 3.5 km/s. The rupture extended from Prince William Sound to the Kenai Peninsula and beyond Kodiak Island.

The Indian Ocean tsunami on December 26, 2004, is considered the worst tsunami in history, causing damage and impacting more than 15 nations bordering the Indian Ocean, [14]. The Sumatra-Andaman earthquake, with a magnitude larger than 9.3, occurred when the Indian Oceanic plate was being subducted beneath the Burma plate and a portion of the Sunda plate, [15].

In the 2004 Sumatra tsunami, MOST calculations indicated a maximum slip height between 5m and 10m, and a close-up of the estimated wave heights in the Bay of Bengal showed a tsunami wave with a height of 70 cm and greater than 2m recorded on the coast of the Bay of Bengal, [16].

Python programming is used to create graphical representations of working tsunami wave models. It is used to calculate the rate at which a tsunami wave spreads for three historical Tsunami events under three different ocean types' wave circumstances.

This paper's first portion examines the several methods currently in use for modeling the rate at which tsunami waves propagate.

The fundamentals of impulse model mathematical formulation are covered in section 2.

Section 3 presents the analysis of historical tsunami events of the homogeneous ocean modules are examined and the outcomes of their simulations results.

The paper is concluded in Section 4.

2 Impulse Model Mathematical Formulation

There are three main phases in the evolution of earthquake-induced tsunami waves: generation, propagation, and run-up. The impulse model employed in this study comprehensively computes all three stages of tsunami waves.

2.1 Tsunami Generation

The impulse model is utilized to simulate a tsunami triggered by an underwater earthquake. During an earthquake, the seafloor experiences movement, leading to a significant displacement of the water above the sea. This displacement is attributed to an impulse force resulting from the release of a considerable quantity of earthquake energy. Assuming the seafloor is initially at rest, with the velocity of the seabed in the x, y, and z directions (u, v, and w) being zero at time t=0, the seabed begins to shift due to the impulse force until it reaches a time known as the rising time required for seabed displacement.

Various forces, including the body force by the fault and the hydrostatic pressure force by saltwater, oppose the seabed's displacement. An impulse force (F) is exerted on the seabed to displace it. The motion of the shifting seabed can be derived using Newton's third law of motion. The formula for calculating the impulsive force (FI) created to shift the seabed is as follows: The body force by the fault and hydrostatic pressure

force by saltwater are the forces opposing the seabed from displacement, an impulse force (F) is exerted on the seabed to displace it. The motion of the shifting seabed can be derived with the use of Newton's third law of motion. The formula for calculating the impulsive force (F_I) created to shift the seabed is as follows:

$$F_I = \frac{\mu A_f}{M_0} * 10^{11.8+1.5M} * 10^{-7} \quad (1)$$

For the purpose of moving the seabed, the rising time (t1) is computed using,

$$t_1 = \frac{S_f * m_s}{F_I} \quad (2)$$

Seabed movement is calculated using the below equations and these are applicable in the following conditions are, the time is $0 \le t \le t1$, the horizontal boundary condition in 'x' direction is $x_1 \le x \le x_1 \pm W_f$.

$$\left.\begin{aligned} m_s a_x &= F_{Ix} \\ \int_0^{t1} du_s &= \frac{F_{Ix}}{\rho_s \Delta V_s} \int_0^{t1} dt \\ m_s a_z &= F_{Iz} - F_g - F_H \\ \int_0^{t1} dw_s &= \left[\frac{F_{Iz}}{\rho_s \Delta V_s} - \frac{\rho_w . g . d_w . \Delta A_w}{\rho_s \Delta V_s}\right] \int_0^{t1} dt \end{aligned}\right\} \quad (3)$$

From Equation (1) to (3), the symbols represent the following:

M: Magnitude of the earthquake

μ: Shear modulus of the earth's crust at the point of generation

A_f: Area of the fault

M_o: Seismic moment

S_f: Fault slip factor

m_s: Seabed mass

F_I: Impulse force

Subscripts 's' and 'w' represent the seabed and seawater, respectively. Symbols include:

m: Mass

ρ: Mass density

V: Volume of the displaced seabed

A: Area

d_w: Average depth of the water

F_{Ix}: Horizontal impulse force

FIz: Vertical impulse force

F_g: Body force

F_H: Hydrostatic pressure force

u, w: Horizontal and vertical velocities in x and z directions

g: Gravity acceleration

Consider a fluid domain in three dimensions that is unbounded in the x, y of horizontal and bounded in z of vertical direction. The domain's initial conditions are (i) fluid equilibrium, (ii) seawater velocity (u = v = w = 0 in x, y, and z directions), and (iii) z = = 0 at the free surface and z = -h near the seafloor. To mimic the creation of tsunami waves more effectively, the momentum change of the seabed is equated to that of the saltwater above it. The governing equations are applicable in the following conditions are,

$-\infty < x < \infty;\ -\infty < y < \infty, -h < z < 0.$

$$\left.\begin{aligned} \nabla . u &= 0 \\ \frac{Du}{Dt} + \frac{1}{\rho}\nabla P + gz &= 0 \end{aligned}\right\} \quad (4)$$

The velocity of seawater due to the seabed and beginning seawater elevation is estimated by deriving the following equation, Because the average water depth is used in this generation region, the velocity doesn't depend on the space dU/ds = 0, U(u, v). The following equations are derived from equation (4) to account for the additional impulse force caused by the bottom moment when determining the velocity of seawater in the x, y, and z directions:

$$\frac{\partial U}{\partial t} + u\frac{\partial U}{\partial x} + v\frac{\partial U}{\partial y} + w\frac{\partial U}{\partial z} - \frac{m_s}{m_w}\frac{\partial U_s}{\partial t} = 0 \quad (5)$$

$$\frac{\partial w}{\partial t} + u(\nabla . w) + \frac{1}{\rho}\frac{\partial P}{\partial z} + g\frac{\partial \eta}{\partial y} - \frac{m_s}{m_w}\frac{\partial w_s}{\partial t} = 0 \quad (6)$$

Equation (5) above is used to get the seawater velocity in the direction of elevation of displaced water in the x and y directions, and equation (6) is used to determine the seawater velocity in the z direction. The calculation for seawater subsidence goes the other way from elevation. To calculate the sinking of seawater, the vertical velocity is multiplied by the gravitational force.

2.2 Tsunami Propagation

After the tsunami was generated, the wave began to spread from a source point in all directions. The tsunami wave travels over very long distances without significantly reducing its energy. This tsunami wave propagation modelling makes use of the solitary wave theory and the Boussinesq wave approximation. This includes the dispersion relationship because the tsunami wave modelling takes into account the changing bathymetry.

The domain boundary is expressed as $\Omega = R^2 \times [-d + \xi(x, y, t), \eta(x, y, t)]$ because the bottom boundary shifts after an earthquake depending on the type of fault. Where, η is the vertical elevation of the sea surface and ξ is the height of the sea bed

deformation. The seafloor is rigid, and impermeable; the flow is irrotational; the fluid is ideal; surface tension is disregarded; the pressure at the free surface is constant; the wave height is minimal in relation to the wave length; and the potential flow theory is applicable. The vertical boundary condition is changes to,

$$-\mathrm{d} + \xi(\mathrm{x},\mathrm{y},\mathrm{t}) \leq \mathrm{z} \leq \eta(\mathrm{x},\mathrm{y},\mathrm{t}).$$

$$\left.\begin{aligned} &\frac{\partial u}{\partial x}+\frac{\partial v}{\partial y}+\frac{\partial w}{\partial z}=0 \\ &\frac{\partial u}{\partial t}+u\frac{\partial u}{\partial x}+v\frac{\partial u}{\partial y}+\frac{1}{\rho}\frac{\partial P}{\partial x}+g\frac{\partial \eta}{\partial x}=0 \\ &\frac{\partial v}{\partial t}+u\frac{\partial v}{\partial x}+v\frac{\partial v}{\partial y}+\frac{1}{\rho}\frac{\partial P}{\partial y}+g\frac{\partial \eta}{\partial y}=0 \end{aligned}\right\} \quad (7)$$

Since the tsunami wave has a long period and the pressure at the free surface is nil, the wave height (H) is smaller than the wavelength (L). Using equation (6) to obtain the pressure changes at the bottom during the earthquake event, vertical acceleration is omitted for the long wave approximation, i.e. Du/Dt = 0, and the force acting on the seawater owing to the displacement of the seabed is applied. The below equation's negative sign denotes a pressure that is greater than the normal pressure as measured at the bottom and acting in an upward vertical direction. The development of tsunamis can be seen in the rising pressure. An early warning system for tsunamis uses a bottom pressure recorder to help determine the bottom pressure when a tsunami is coming.

$$P(x,y,-d,t) = -\left[\rho g(\eta - z) + \frac{F_{IZ}(x,y,-h,t)}{\rho.A}\right] \quad (8)$$

3 Analysis of Historical Tsunami Events

The following information is needed for this Impulse modelling study. These information pertains to earthquake, tsunami, and ocean bathymetry. The General Bathymetric Chart of the Oceans (GEBCO), the National Oceanic and Atmospheric Administration (NOAA), and the United States Geological Survey provided the data on bathymetry, earthquake, and tsunami events, respectively. Here, the origin is assumed to be the earthquake epicenter. The distance from the epicenter is indicated by the length in latitude and longitude.

The fault boundary line is mathematically determined using the curve fitting approach, which aids in discretizing the fault line into intervals based on rupture velocity. The sea surface deformation can be calculated by using the estimated seabed deformation in both the horizontal and vertical directions provided by the impulse force. The rise in water level on the ocean side, which spreads as a far-off tsunami, and the decline in water level on the shoreside which propagates as a close-by tsunami, are both examples of this sea surface deformation. Seabed movement causes the sea surface to be raised in the direction of overriding; the height of the elevation is a function of the water depth at the fault location and the impulsive force brought on by the seabed movement.

When a tsunami first rises, it resembles an N-type wave and is characterized by uplift on the ocean side (Distant tsunami) and downward dips on the beach side (local tsunami). The vertical velocity will be zero if the water is displaced to its maximum height. Here, it is assumed that the point of maximal water displacement marks the beginning of the tsunami's spread in directions orthogonal to that of the rupture. As a result, an equal amount of the potential energy of the displaced water is transferred, which is the energy that will cause the tsunami wave to propagate further. Assumes the fluid moves in all eight directions from the commencement point as a result of the energy being distributed in a circular pattern.

Once the tsunami starts, it disrupts the entire ocean's depth, and this wave propagates alone (in shallow water, a wave's wavelength is greater than the depth of the water). The water depth along the path of the tsunami wave propagation affects the wave properties (wave height, amplitude, and wavelength) for shallow-water waves. There are no obstructions in the tsunami wave's path in this wave propagation zone. As a result, it is regarded as a homogenous situation with a variable ocean floor. Every node calculates the wave properties and the interval spacing of 500 m. assuming the tsunami wave propagated as a solitary wave and was driven by the energy of displaced water transferred to the water molecules. Using the linear frequency dispersion relationship, the wavelength and wave period may be calculated. The depth of the sea determines the height of a tsunami wave. The increasing water depth causes the tsunami wave height to decrease towards the ocean. But at the coast, tsunami wave height increases with the reducing water depth.

In this paper, the generation and propagation phases of tsunami were analyzed in detail. The following results are anticipated from the impulse modelling:

(i) Data on seabed deformation;
(ii) Properties of deep-ocean tsunami waves;
(iii) Tsunami wave characteristics at the shore;
(iv) Travel duration of the tsunami wave to reach the destination; and
(v) Tsunami wave's earliest arrival time.

In this study, the three ocean basins where earthquake tsunamis occur most frequently—the Pacific Ocean, Atlantic Ocean, and Indian Ocean—are used to test the applicability of the Impulse modelling method. In order for the tsunamis to affect as many nations as possible across the three continents of Asia, Europe, and North America, tsunami wave propagation analyses were conducted. In this paper, the following historical tsunami events are analyzed:

1. 1755 Lisbon tsunami
2. 1964 Alaska tsunami
3. 2004 Sumatra tsunami

Table 1. Symbols used in this paper, [17]

Sl. No.	Symbols	Names
1	Lon	Longitude
2	Lat	Latitude
3	L_R	Rupture length
4	T_R	Rupture time
5	dS	Slip variation along the fault
6	H_o	Tsunami wave height in the deep ocean
7	C	Wave celerity
8	L	Wave length
9	T	Wave period
10	D	Distance b/n source and destination
11	ETH	Estimated tsunami height at coast
12	ETT	Estimated tsunami travel time
13	EAT	Estimated arrival time of tsunami
14	OTH	Observed tsunami wave height at coast
15	OTT	Observed tsunami travel time
16	ΔH	Difference b/n observed and estimated tsunami height at coast
17	ΔT	Difference b/n observed and estimated tsunami travel time

Table 1 shows the symbols and names of T-impulse model for tsunami wave.

3.1 1755 Lisbon Earthquake

The Great Lisbon earthquake struck Portugal, the Iberian Peninsula, and Northwest Africa on November 1 at approximately 9:40 local time. Everything close by was nearly completely destroyed by the earthquake's aftermath, including subsequent flames and a wave. Seismologists believe the Lisbon earthquake had a magnitude of 7.7 or higher and had its epicenter in the Atlantic Ocean around 200 km west-southwest of tip St. Vincent, a tip in the Algarve region, and about 290 km southwest of Lisbon. It was the city's third known large-scale earthquake in chronological order (after those of 1321 and 1531). Approximately 12,000 people are thought to have died in Lisbon, making it one of the worst earthquakes in recorded history.

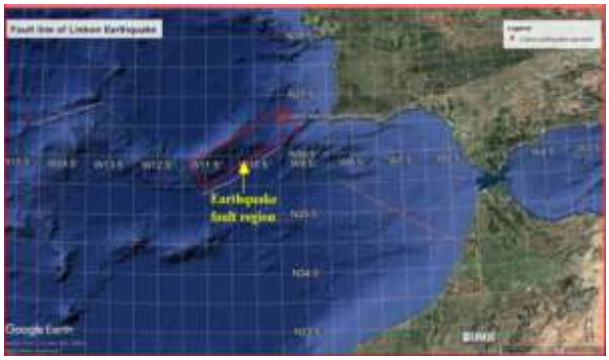

Fig. 2: Modelling study area of the 1755 Lisbon Earthquake

Figure 2 shows the modelling study area of the 1755 Lisbon earthquake, the line indicates the plate boundary between the Eurasian plate and African plate, the red mark indicates the Lisbon earthquake epicenter, and rectangular region shows tsunami generation zone. The earthquake's epicenter is located at 37.00 ^{0}N and 10.00 ^{0}W. The rupture proceeded with a speed of 1.7 km/s westward and took 3 1/2 to 6 minutes to go 360 km rupture length.

Table 2. Earthquake information data for the 1755 Lisbon earthquake tsunami (U.S. Geological Survey)

Sl. No.	Parameters	Values
1	Date	1/11/1755
2	Initiation time	09:30:00 UTC
3	Source	Lisbon, Portugal
4	Epicentre	10.00^{0}W, 37.00^{0}N
5	Magnitude	8.5
6	Focal depth	8 km
7	Fault length	360 km
8	Fault width	80 km
9	Dip angle	40°
10	Rupture duration	3 ½ to 6 minutes

Table 2 shows information about the earthquake that caused a tsunami wave on November 1, 1755 in Lisbon, Portugal collected from the U. S. geological survey. Table 3 shows the estimated values of tsunami-generating parameters in the 1755, Lisbon tsunami. The slip of the fault is estimated by Kannamori

calculations to be 81.938 m for a dip value of 40°. Near the epicenter 52.67 m maximum vertical displacement of the fault was calculated.

On the south side, it is determined that the maximum height of the seafloor increase and the horizontal displacement are 52.67 m and 62.76 m, respectively. The propagated tsunami waves were travel in the Atlantic Ocean region.

Table 3. 1755 Lisbon earthquake – Estimated values of tsunami generating parameter

Sl. No.	Parameters	Values	Units
1	Earthquake energy	3.55E+17	J
2	Seismic Moment	7.08E+21	Nm
3	Impulse force	4.33E+15	N
4	Slip	52.66884	M

Figure 3 shows the fault boundary coordinates of Lisbon earthquake fit to the curve to discretize the fault line in the interval spacing 1.7 km depending on the rupture velocity (v = fault length/rupture duration or 360/211.75 = 1.7) to find the earthquake fault zone where the tsunami waves are generated. Using the discretization helps to find the fault slip variation along the fault boundary line that indicates in Figure 4 for the 1755, Lisbon earthquake.

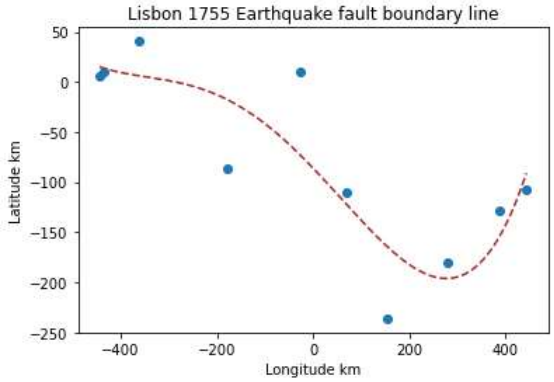

Fig. 3: 1755 Lisbon earthquake fault boundary line with curve fitting

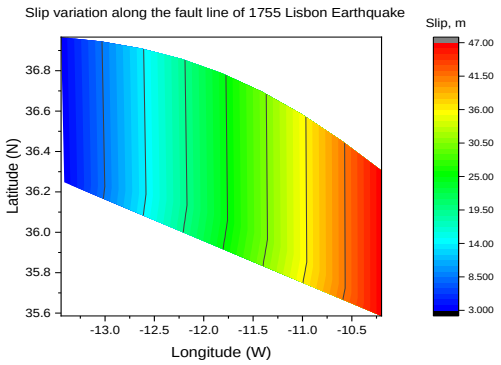

Fig. 4: Fault slip variation along the Lisbon earthquake fault boundary line

The Lisbon Earthquake (1/11/1755) was initiated at the time of 09 hours 30 minutes UTC. The rupture begins at the epicenter (10.00 ^{0}W, 37.00 ^{0}N). Rupture propagate westward in the fault boundary, It took 211.75 seconds to reach the rupture length of 359.9 km. The total time for rupture is estimated as 211.75 seconds or 3 minutes 31 seconds, and the slip variation near the epicenter is a maximum of 52.67 m and it varies along the fault between 3 m and 52.67 m (U. S. Geological Survey) that given in Table 4.

Table 4. The seabed deformation along the fault boundary line of 1755 Lisbon Earthquake

Nodes	Lat (°N)	Lon(°W)	L_R, km	T_R, s	dS, m
1	36.305	10.200	39.99	23.52	46.81
2	36.453	10.603	79.33	46.67	41.06
3	36.584	11.008	117.9	69.38	35.41
4	36.696	11.413	155.8	91.67	29.86
5	36.788	11.819	193.1	113.6	24.41
6	36.858	12.225	229.9	135.2	19.03
7	36.910	12.632	266.3	156.6	13.69
8	36.944	13.038	302.6	178.0	8.394
9	36.96	13.445	338.7	199.2	3.108

Table 5 depicts the destination that is selected for this modelling to analyze the behavior of tsunami waves. The deep ocean tsunami wave characteristics caused by the Lisbon earthquake in 1755 are shown in Table 6. In the deep ocean, a tsunami's wave height is estimated to be between 0.4 and 1.13m, its propagation speed is calculated to be between 84 and 195 km per second, its wavelength is calculated to be between 70 and 1050 km, and its period is calculated to be between 14 minutes and 1 hour 30 minutes.

Table 5. Selected destination for this modeling

Sl. No.	Location
1	Portugal-Azores
2	Penzance, England
3	Mounts Bay, England
4	Gibraltor, Spain
5	Hayle, England

Table 6. Characteristics of the first tsunami wave to arrive at the destinations in the 1755 Lisbon tsunami

Location	Lat (ºN)	Lon (ºW)	H_o, m	C, km/s	T, hh/mm/ss
1	38.72	27.22	1.14	187.4	0.52.49
2	50.117	5.55	0.81	103.6	0.19.08
3	50.033	5.417	0.66	84.97	0.14.12
4	36.15	5.35	0.47	195.9	1.30.04
5	50.167	5.417	0.73	93.71	0.16.30

Table 7 shows the results of the first tsunami wave to reach the defined destination by using the Impulse modelling for 1755, Lisbon earthquake tsunami. From the historical data, the tsunami wave height at the coast of locations given in the table is obtained. By comparing the results of historical observed data with the estimated data shows the Impulse modelling study can be applied to real-time tsunami events to determine the tsunami wave behavior.

Table 7. The initial tsunami wave's outcomes at the coastline of the destinations in the 1755 Lisbon tsunami

Location	D, km	ETH, m	ETT, hh/mm/ss	EAT, hh/mm/ss
1	1512	1.972	2.49.13	12.19.52
2	1576.8	2.876	2.14.31	11.44.31
3	1571.9	2.352	2.13.25	11.43.25
4	417.80	1.951	1.20.05	10.50.05
5	1585.9	1.740	2.28.11	11.58.11

The link between the historical and estimated tsunami wave height at each location from the 1755 Lisbon earthquake is shown in Table 8.

The table shows that there is a very tiny, potentially inconsequential, discrepancy between historical and estimated tsunami wave heights near the shore, which can be corrected in the future. The average percentage of accuracy of estimated values is obtained as 86.38%.

Table 8. Relationship between the historical (NOAA) and estimated 1755 Lisbon earthquake-tsunami wave height at the destinations

Location	OTH, m	ETH, m	ΔH, m	Accuracy (%)
1	2	1.9722	0.028	98.61
2	2.44	2.8761	0.436	82.127
3	1.8	2.3528	0.553	76.5046
4	2.1	1.9518	0.148	92.9429
5	2.13	1.7406	0.389	81.7183

Figure 5 presents a comparison graph between the historical and estimated tsunami wave heights for the Lisbon tsunami of 1755, reaching different destinations. Numerical numbers on the graph correspond to the locations indicated in the table. Historical tsunami wave height information along the coast is derived from NOAA data. The graph aims to illustrate the effectiveness of the Impulse model in predicting the behavior of the tsunami wave during the actual occurrence.

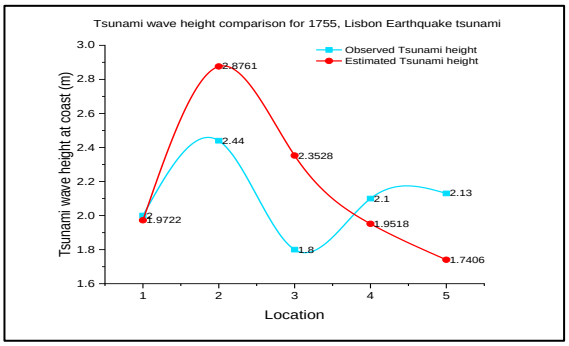

Fig. 5: Comparison graph between the historical and estimated tsunami wave height at the destinations due to the 1755-Lisbon Earthquake-tsunami

3.2 1964 Alaska Earthquake

The 9.2-magnitude Prince William Sound earthquake on March 28, 1964, now the second-largest earthquake ever recorded, was the easternmost megathrust earthquake. The earthquake ruptured along a fault line approximately 800 miles (1,300 km) long. The event's rupture length extended approximately 700 km from Prince William Sound in the northeast to the southern tip of Kodiak Island in the southwest.

This seismic activity occurred in the area where the North American plate subducts beneath the Pacific plate, giving rise to the Aleutian Islands and the deep offshore Aleutian Trench through subduction. Additionally, this megathrust earthquake triggered a destructive tsunami, causing damage along the Gulf of Alaska, the US West Coast, and in Hawaii.

Fig. 6: Modelling study area of the 1964 Earthquake

Figure 6 shows the modelling study area of the 1964 Alaska earthquake, the line indicates the Aleutian arc which is a plate boundary between the North America plate and Pacific plate, the yellow mark indicates the Alaska earthquake epicenter, and rectangular region shows tsunami generation zone. The earthquake's epicenter is located at 61.017 ^{0}N and 147.648 ^{0}W. The rupture proceeded with a speed of 1.4 - 2 km/s in the southwest direction and took 6 minutes 51 seconds to go 699.6 km rupture length.

Table 9. Earthquake information data for the 1964 Alaska earthquake tsunami (U.S. Geological Survey)

Sl. No.	Parameters	Values
1	Date	28/3/1964
2	Initiation time	3:36:14 UTC
3	Source	Alaska
4	Epicenter	61.017°N, 147.648°W
5	Magnitude	9.2
6	Focal depth	33 km
7	Fault length	700 km
8	Dip angle	6 – 12°
9	Rupture velocity	1.4 – 2 km/s

Table 9 shows information about the earthquake that caused a tsunami wave on March 28, 1964 in Alaska collected from the U. S. geological survey.

Table 10 shows the estimated values of tsunami-generating parameters in the 1964, Alaska tsunami. The slip of the fault is estimated by Kannamori calculations to be 114.62 m for a dip value of 9°. Near the epicenter 17.93 m maximum vertical displacement of the fault was calculated. The rupture propagated towards the westward direction, the South Pacific plate is subducted under the North American plate. It is determined that the maximum height of the seafloor increase and the horizontal displacement are 17.93 m and 113.21 m, respectively. The propagated tsunami waves were traveling in the Atlantic Ocean region.

Table 10. 1964 Alaska earthquake – Estimated values of tsunami generating parameter

Sl. No.	Parameters	Values	Units
1	Earthquake energy	3.98E+18	J
2	Seismic Moment	7.94E+22	Nm
3	Impulse force	3.47E+16	N
4	Slip	17.93	m

Figure 7 shows the fault boundary coordinates of Alaska earthquake fit to the curve to discretize the fault line in the interval spacing of 1.7 km depending on the rupture velocity to find the earthquake fault zone where the tsunami waves are generated. Using the discretization helps to find the fault slip variation along the fault boundary line that indicates in Figure 8 for the 1964, Alaska earthquake.

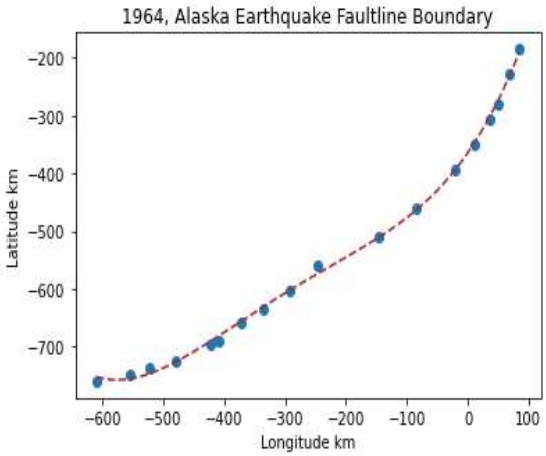

Fig. 7: 1964 Alaska earthquake fault boundary line with curve fitting

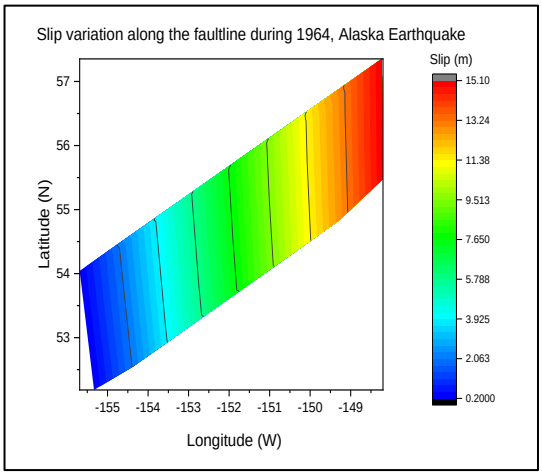

Fig. 8: Fault slip variation along the Alaska earthquake fault boundary line

The Alaska Earthquake (28/3/1964) was initiated at the time of 03 hours 36 minutes 14 seconds UTC. The rupture begins at the epicenter

(147.648 ^{0}W, 61.017 ^{0}N). Rupture propagate westward in the fault boundary, It took 411.47 seconds to reach the rupture length of 699.59 km. The total time for rupture is estimated as 411.47 seconds or 6 minutes 51 seconds, and the slip variation near the epicenter is a maximum of 17.93 m and it varies along the fault between 0.2 m and 17.93 m (U. S. Geological Survey) given in Table 11.

Table 11. The seabed deformation along the fault boundary line of 1964 Alaska Earthquake

Nodes	Lat (ºN)	Lon (ºW)	L_R, km	T_R, s	dS, m
1	57.353	148.231	110.70	65.12	15.10
2	56.703	149.367	200.89	118.17	12.78
3	56.226	150.477	283.89	166.99	10.66
4	55.801	151.565	366.08	215.34	8.55
5	55.358	152.628	449.99	264.70	6.40
6	54.883	153.663	534.99	314.70	4.23
7	54.414	154.677	617.15	363.03	2.12
8	54.043	155.688	691.67	406.86	0.21

Table 12 depicts the destination that is selected for this modelling to analyze the behavior of tsunami waves. The deep ocean tsunami wave characteristics resulting from the Alaska earthquake in 1964 are presented in Table 10. In deep ocean conditions, the estimated tsunami wave height ranges from 0.42 to 48 meters, the calculated propagation speed ranges between 22 and 218 kilometers per second, the wavelength is estimated to be between 218 and 225 kilometers, and the wave period is calculated to be between 10 and 15 minutes.

Table 12. Selected destination for this modelling

Sl. No.	Location
1	Cape St Elias
2	Cape Chiniak
3	Kodiak Island
4	Old Harbor Kodiak
5	Cape Yakataga
6	Yakutat

Table 13. Characteristics of the first tsunami wave to arrive at the destinations in the 1964 Alaska tsunami, [17], [18], [19]

Location	Lat (ºN)	Lon (ºW)	C, km/s	L, km	T, hh/mm/ss
1	59.8	144.6	218.7	142.41	0.10.51
2	57.621	152.1	224.4	157.44	0.11.41
3	57.718	152.5	223.7	175.10	0.13.02
4	57.201	153.3	222.9	196.83	0.14.42
5	60.07	142.4	219.2	143.34	0.10.53
6	59.55	139.7	219.2	143.47	0.10.54

Table 13 depicts the distance and time reached the first tsunami wave arrived in the destinations using Latitude and Longitude in the 1964 Alaska tsunami.

Table 14. The initial tsunami wave's outcomes at the coastline of the destinations in the 1964 Alaska tsunami

Location	D, km	ETH, m	ETT, hour	EAT, hh/mm/ss
1	283.4886	1.4	0.62	4.13.16
2	164.574	9.57	0.55	4.09.16
3	184.2267	6.3	0.723	4.19.37
4	157.6422	7.4	0.74	4.20.26
5	383.8488	3.89	0.83	4.26.08
6	472.7035	1.5	1.17	4.53.34

Table 14 shows the results of the first tsunami wave to reach the defined destination by using the Impulse modelling for 1964, Alaska earthquake tsunami. From the historical data, the tsunami wave height at the coast of locations given in the table is obtained. By comparing the results of historical observed data with the estimated data shows the Impulse modelling study can be applied to real-time tsunami events to determine the tsunami wave behavior.

The connection between historical and estimated tsunami travel times to reach specified locations from the 1964 Alaska earthquake tsunami is illustrated in Table 12. The table indicates a minimal, potentially inconsequential, discrepancy between historical and estimated tsunami wave heights near the shore, which could be addressed in future corrections. The average percentage accuracy of estimated values is calculated as 88.87%.

Table 15. Relationship between the historical (NOAA) and estimated 1964 Alaska earthquake-tsunami wave travel time to reach destinations

Location	OTT (hours)	ETT (hours)	ΔT, mm/ss	Accuracy (%)
1	0.7	0.62	4.48	88.5714
2	0.5	0.55	3.00	90
3	0.8	0.723	4.37	89.3499
4	0.8	0.74	3.36	92.5
5	0.7	0.83	7.48	81.4286
6	1.4	1.28	7.12	91.4286

Figure 9 presents a comparison graph between the historical and estimated tsunami travel times for the Alaska tsunami of 1964 to reach various destinations. Numerical numbers on the graph correspond to the locations indicated in the table. Historical tsunami wave height information along the coast is derived from NOAA data. The graph aims to illustrate the effectiveness of the Impulse

models in predicting the behavior of the tsunami wave during the actual occurrence.

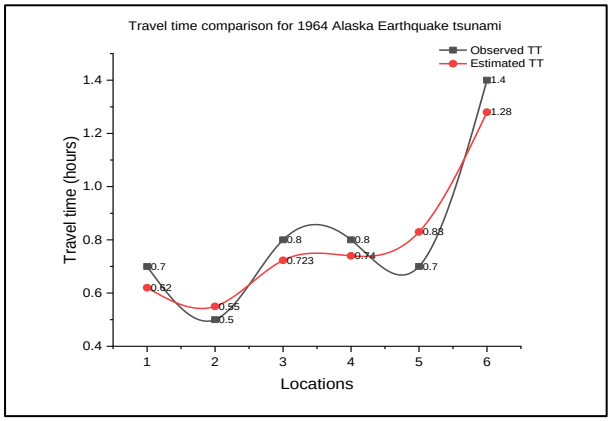

Fig. 9: Comparison graph between the historical and estimated tsunami wave travel time to reach the destinations due to the 1964-Alaska earthquake-tsunami

3.3 2004 Sumatra Andaman Earthquake

The seafloor on the underlying Burma plate ruptured in a northward direction during the Sumatra-Andaman earthquake of 2004, elevating seaward into the trench and subsiding landward towards the shoreline. The rupture extended from northwest Sumatra north to the Andaman Islands. The earthquake's epicenter is approximately 110 to 130 meters from the fault boundary at 3.316°N and 95.854°E. The rupture travelled a distance of 1200 kilometers in 8 to 10 minutes at a pace of 2.5 km/s towards the north.

Fig. 10: Modelling study area of the 2004 Sumatra-Andaman Earthquake

Figure 10 depicts the modeling study area of the 2004 Off West Coast of Sumatra earthquake. The red line indicates the plate boundary between the Burma plate and the Indian plate, the red mark signifies the Sumatra earthquake epicenter, and the rectangular region outlines the tsunami generation zone or earthquake fault zone. The earthquake's epicenter is situated at 3.3160°N and 95.8540°E. The rupture advanced at a speed of 2.5 km/s in the Northward direction and took 7 minutes and 59 seconds to cover a rupture length of 1199.87 km.

Table 16 shows information about the earthquake that caused a tsunami wave on December 26, 2004 in the Off West Coast of Sumatra collected from the U. S. geological survey.

Table 16. The seabed deformation along the fault boundary line of 2004 Sumatra Earthquake

Sl. No.	Parameters	Values
1	Date	26/12/2004
2	Initiation time	00:58:53.4 UTC
3	Source	Off West Coast of Sumatra
4	Epicentre	3.316ºN, 95.854ºE
5	Magnitude	9.15
6	Focal depth	30 km
7	Fault length	1200 km
8	Dip angle	8º
9	Rupture velocity	2.5 km/s

Table 17 shows the estimated values of tsunami-generating parameters in the 2004 Sumatra, Indian Ocean tsunami. The slip of the fault is estimated by Kannamori calculations to be 61.88 m for a dip value of 8º. Near the epicenter 8.61 m maximum vertical displacement of the fault was calculated. The rupture propagated towards the northward direction, the Indian plate in west side is subducted under the Burma plate in east side. It is determined that the maximum height of the seafloor increase and the horizontal displacement are 8.61 m and 61.88 m, respectively. The propagated tsunami waves were traveling in the Atlantic Ocean region.

Table 17. 2004 Sumatra earthquake – Estimated values of tsunami generating parameter

Sl. No.	Parameters	Values	Units
1	Earthquake energy	3.35E+18	J
2	Seismic Moment	6.68E+22	Nm
3	Impulse force	5.41E+16	N
4	Slip	8.612	m

Figure 11 illustrates the fault boundary coordinates of the Sumatra earthquake, fitted to a curve and discretized at interval spacings of 2.5 km. This discretization is based on the rupture velocity and is crucial for identifying the earthquake fault zone where tsunami waves are generated. The process of discretization aids in determining the fault slip variation along the fault

boundary line, as indicated in Figure 12 for the 2004 Sumatra earthquake.

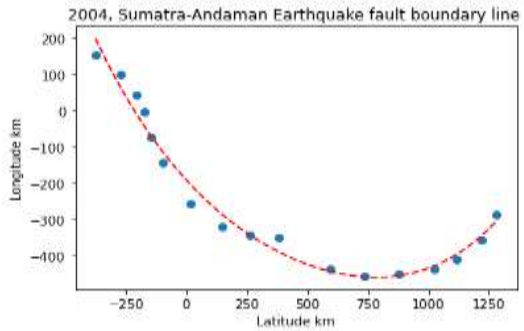

Fig. 11: 2004 Sumatra earthquake fault boundary line with curve fitting

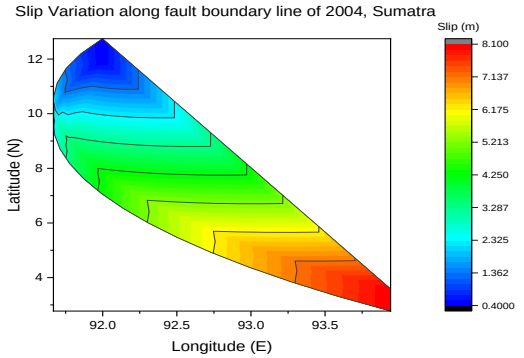

Fig. 12: Fault slip variation along the Sumatra earthquake fault boundary line

The Off West Coast of Sumatra Earthquake on December 26, 2004, was initiated at 58 minutes 53.4 seconds UTC. The rupture commenced at the epicenter (95.8540E, 3.3160N) and propagated northward along the fault boundary. It took 479.94 seconds to reach a rupture length of 1199.87 km. The total time for rupture is estimated to be 479.4 seconds or 7 minutes and 59 seconds. The slip variation near the epicenter is a maximum of 8.61 m, and it varies along the fault between 0.4 m and 8.61 m, as reported by the U.S. Geological Survey (shown in Table 15).

Table 18. The seabed deformation along the fault boundary line of 2004 Sumatra Earthquake

Nodes	Lat (ºN)	Lon(ºW)	L_R, km	T_R, s	dS, m
1	3.853	93.773	143.57	57.43	7.582
2	4.930	93.132	279.04	111.6	6.610
3	6.007	92.623	408.73	163.4	5.679
4	7.084	92.227	534.32	213.7	4.778
5	8.161	91.938	657.01	262.8	3.897
6	9.238	91.753	777.81	311.12	3.030
7	10.31	91.679	897.87	359.15	2.168
8	11.39	91.733	1018.8	407.54	1.300
9	12.47	91.938	1143.3	457.34	0.407

Table 19 depicts the destination that is selected for this modelling to analyze the behavior of tsunami waves. The deep ocean tsunami wave characteristics caused by the Sumatra earthquake in 1964 are shown in Table 20. In the deep ocean, a tsunami's wave height is estimated to be between 0.3 and 3.17 metress, its propagation speed is calculated to be between 150 and 190 kilometres per second, its wavelength is calculated to be between 300and 450 kilometres, and its period is calculated to be between 16 minutes and 1 hour 57 minutes.

Table 19. Selected destination for this modeling

Sl. No.	**Location**
1	Portblair,AndamanIsland
2	Marina, Chennai
3	Silver beach, Cuddalore
4	Velankanni
5	Nagapattinam
6	Karaikal, Puducherry
7	Appikonda beach, Vizag
8	Paradeep, Orissa
9	Cocos island, Australia

Table 20. Characteristics of the first tsunami wave to arrive at the destinations in the 2004, Sumatra tsunami

Location	**Lat (ºN)**	**Lon (ºW)**	**C, km/s**	**L, km**	**T, hh/mm/ss**
1	11.675	92.761	159.102	306.91	0.32.09
2	13.083	80.3	179.034	436.44	0.40.37
3	11.739	79.786	181.086	422.67	0.38.54
4	10.681	79.853	181.729	376.66	0.34.32
5	10.784	79.850	184.389	337.10	0.30.28
6	10.918	79.853	183.019	340.73	0.31.01
7	17.567	83.171	147.873	15748	5.35.01
8	20.26	86.7	147.141	15516	5.17.30
9	-12.12	96.883	84.901	32.77	0.06.25

Table 21 displays the results of the time for the first tsunami wave to reach the defined destination using the Impulse modeling for the 2004 Sumatra earthquake tsunami. Historical data provides the observed tsunami wave height at the coast of locations given in the table.

Comparing the results of historical observed data with the estimated data shows that the Impulse modeling study can be applied to real-time tsunami events to determine the tsunami wave behavior.

Table 21. The initial tsunami wave's outcomes at the coastline of the destinations in the 2004 Sumatra tsunami

Location	D, km	ETH, m	ETT, hour	EAT, (UTC) hh/mm/ss,
1	103.8795	2.3	0.35	1.19.53
2	1287.243	2.18	2.48	3.27.41
3	1328.997	6.17	2.35	3.19.53
4	1316.846	3.85	2.57	3.33.05
5	1317.385	12.47	2.47	3.27.05
6	1317.424	5.16	2.36	3.20.29
7	1114.084	1.9	2.513	3.29.39
8	979.0124	1.572	2.47	3.27.05
9	1744.476	0.7	2.3386	3.19.11

The connection between historical and estimated tsunami travel times to reach defined locations from the 2004 Sumatra earthquake tsunami is illustrated in Table 18. The table indicates a very slight, potentially inconsequential discrepancy between historical and estimated tsunami wave heights near the shore, which can be addressed in the future. The average percentage accuracy of estimated values is calculated as 93.48%.

Table 22. Relationship between the historical (NOAA) and estimated 2004 Sumatra earthquake-tsunami wave travel time to reach destinations-[18], [19], [20]

Location	OTT (hours)	ETT (hours)	ΔT, mm/ss	Accuracy (%)
1	0.25	0.35	6.00	60
2	2.567	2.48	5.13	96.6108
3	2.31	2.35	2.24	98.2979
4	2.51	2.57	3.36	97.6096
5	2.516	2.47	2.45	98.1717
6	2.27	2.36	5.24	96.0352
7	2.6	2.513	5.13	96.6538
8	2.46	2.47	0.36	99.5935
9	2.3	2.3386	2.18	98.3494

Table 22 depicts the accuracy of the estimated tsunami wave travel time of 2004-Sumatra earthquake as compared to the Observed tsunami travel time.

The comparison graph between the historical and estimated tsunami travel times for the Sumatra, Indian Ocean tsunami of 2004 to reach various destinations is depicted in Figure 13. Numerical numbers on the graph correspond to the locations indicated in the table. NOAA data is utilized for historical tsunami wave height information along the coast. The outcomes demonstrate the effectiveness of the Impulse models in predicting the behavior of the tsunami wave during the actual tsunami occurrence.

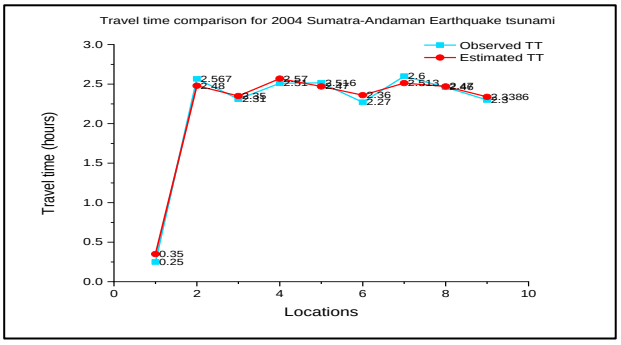

Fig. 13: Comparison graph between the historical and estimated tsunami wave travel time to reach the destinations due to the 2004, Sumatra earthquake-tsunami

4 Conclusion

The Impulse modeling method, employed to simulate the tsunami generation and propagation phases, is utilized to analyze three significant historical tsunami events: the 1755 Lisbon tsunami, the 1964 Alaska tsunami, the 2004 Sumatra tsunami. The run-up phase of the tsunami is not explored due to a lack of historical data in this context. These three historical tsunamis, occurring in various regions, cover six continents (Asia, Europe, North America), three oceans (the Pacific, Atlantic, and Indian Oceans), and numerous nations, providing a comprehensive test of the applicability and suitability of the impulse modeling approach across diverse oceanic regions.

The study examines the tsunami wave characteristics during the propagation phase using Impulse modeling and observes that these characteristics are solely dependent on the ocean's depth, with earthquake parameter variations having no impact on tsunami wave propagation properties. The accuracy of the results is assessed by comparing them with historical data obtained from the U.S. Geological Survey and the National Oceanic and Atmospheric Administration (NOAA). The overall accuracy is determined to be 90.25%. The accuracy percentage is higher for distant tsunamis and lower for local or near shore tsunamis but remains within an acceptable range.

The Impulse modeling method proves effective in forecasting tsunami wave behavior across various oceanic regions, even with minimal earthquake data. Reliable results are obtained in homogeneous ocean conditions when there are no obstructions in the path of the tsunami wave.

However, caution is advised when applying the method in conditions with obstacles. Future research aims to enhance the accuracy of Impulse modeling across all ocean conditions.

References:

[1] Helene and M T Yamashita (2006), Understanding the tsunami with a simple model, *European Journal of Physics*, 27,855–863.

[2] Smid, T. C. (1970). Tsunamis in Greek Literature. *Greece and Rome*, 17(01), 100–104, https://doi.org/10.1017/S0017383500017393.

[3] Pablo G. Silva a, Javier Elez b, Raúl Pérez-López c, Jorge Luis Giner-Robles d, Pedro V. Gómez-Diego a, Elvira Roquero e, Miguel Ángel Rodríguez-Pascua c, Teresa Bardají f (2023), The AD 1755 Lisbon Earthquake-Tsunami: Seismic source modelling from the analysis of ESI-07 environmental data, *Quaternary International*, 651, 6-24.

[4] Chris Zweck a 1, Jeffrey T Freymueller a, Steven C Cohen b (2002), The 1964 great Alaska earthquake: present day and cumulative postseismic deformation in the western Kenai Peninsula, *Physics of the Earth and Planetary Interiors*, 132,(1–3), 5-20.

[5] Chris Zweck, Jeffrey T. Freymueller, Steven C. Cohen (2002). Three-dimensional elastic dislocation modeling of the postseismic response to the 1964 Alaska earthquake. *Journal of Geophysical Research: Solid Earth*, 107(B4), ECV 1–1–ECV 1–11.

[6] Alexander B. Rabinovich, Rogério N. Candella & Richard E. Thomson (2011) "Energy Decay of the 2004 Sumatra Tsunami in the World Ocean". *Pure Appl. Geophys.*, 168, 1919–1950.

[7] Robert L. Long (1965) On the Boussinesq approximation and its role in the theory of internal waves, *Tellus*, 17, 1, 46-52, https://doi.org/10.1111/j.2153-3490.1965.tb00193.x.

[8] Kanamori, H. (1977) The energy release in great earthquakes, *J. Geophys. Res.*, 82, 2981 – 2987.

[9] Fred E. Camfield (1994), Tsunami Effects on Coastal Structures, *Journal of Coastal Research*, Special Issue No. 12. Coastal Hazards: Perception, Susceptibility and Mitigation (1994), pp. 177-187

[10] Furumoto, A. S., Analysis of Rayleigh wave, part II, in Source Mechanism Study of the Alaska Earthquake and Tsunami of March 27, 1964, Rep. HIG-65-17, pp. 31 – 2, Univ. of Hawaii, *Inst. of Geophys.*, Honolulu, Dec. 1965

[11] Kanamori, H., The Alaska earthquake of 1964: Radiation of long-period surface waves and source mechanisms, *J. Geophys. Res.*, 75, 5029 – 5040, 1970.

[12] George Pararas-Carayannis (2018), Brief History of Early Pioneering Tsunami Research – Part A, *Journal of Tsunami Society International*, Vol. 37, 1-11.

[13] Max Wyss;James and N. Brune (1967) The Alaska earthquake of 28 March 1964: A complex multiple rupture, *Bulletin of the Seismological Society of America*, (1967), 57 (5), pp.1017–1023.

[14] Anawat Suppasri, Kazuhisa Goto, Abdul Muhari, Prasanthi Ranasinghe, Mahmood Riyaz, Muzailin Affan, Erick Mas, Mari Yasuda & Fumihiko Imamura (2015), A Decade After the 2004 Indian Ocean Tsunami: The Progress in Disaster Preparedness and Future Challenges in Indonesia, Sri Lanka, Thailand and the Maldives, *Pure and Applied Geophysics*, 172, 3313–3341.

[15] Eric L. Geist & Tom Parsons (2006), Probabilistic Analysis of Tsunami Hazards*, *Natural Hazards*, vol. 37, pp.277–314.

[16] Vasily Titov, Alexander B. Rabinovich, Harold O. Mofjeld, Richard E. Thomson, And Frank I. Gonza´ez (2005), The Global Reach of the 26 December 2004 Sumatra Tsunami, *Science*, Vol. 309, Issue 5743,pp. 2045-2048

[17] NOAA. NCEI / WDS Global Historical Tsunami Database of 1964 Alaska earthquakes and tsunami, [Online]. https://www.ngdc.noaa.gov/hazel/view/hazards/tsunami/related-runups/1954 (Accessed Date: February 16, 2024).

[18] NOAA. The tsunami source data is related to tsunami run-up data observed - 2004 Indian Ocean earthquake and tsunami, [Online]. https://www.ngdc.noaa.gov/hazel/view/hazards/tsunami/related-runups/2439 (Accessed Date: February 16, 2024).

[19] National Geophysical Data Center / World Data Service: NCEI/WDS Global Historical

Tsunami Database.- NOAA National Centers for Environmental Information. doi: 10.7289/V5PN93H7

[20] The General Bathymetric Chart of the Oceans - bathymetric data sets of world's oceans, [Online]. https://www.gebco.net/data_and_products/gridded_bathymetry_data/ (Accessed Date: February 16, 2024).

Contribution of Individual Authors to the Creation of a Scientific Article (Ghostwriting Policy)

- Syed Mohamed has carried out the following:
  - Identified the parameters
  - Developed the theory and performed the computations.
  - Verified the analytical methods
  - Conceived the original idea.
  - Developed the theoretical formalism, performed the analytic calculations and performed the numerical simulations
  - Carried out the statistical, mathematical, computational techniques to analyze the historical and study data.
  - Carried out the simulation and the optimization.
  - Designed the model and the computational framework and analysed the data
  - Carried out the implementation
  - Worked out almost all of the technical details, and performed the numerical calculations for the suggested experiment.

- Pon Selvam has carried out the following:
  - Encouraged
  - Helped suggestion given in the articles

Both authors contributed to the final version of the manuscript

Sources of Funding for Research Presented in a Scientific Article or Scientific Article Itself

No funding was received for conducting this study.

Conflict of Interest

The authors have no conflicts of interest to declare.